Supplementary Information

Cascade Detection of Pyridoxal 5'-Phosphate and Al^{3+} Ions Based on Dual-Functionalized Red-Emitting Copper Nanoclusters

Vinita Bhardwaj[a], Shilpa Bothra[a], Yachana Upadhyay[b] and Suban K Sahoo[a]*

[a] Department of Chemistry, Sardar Vallabhbhai National Institute Technology, Surat-395007, Gujarat, India. E-mail: sks@chem.svnit.ac.in; Tel: +91-9723220556.
[b] Department of Chemistry, Malaviya National Institute of Technology, Jaipur-302017, Rajasthan, India.

Contains 13 pages: 14 Supporting Figures, and 1 supporting Table.

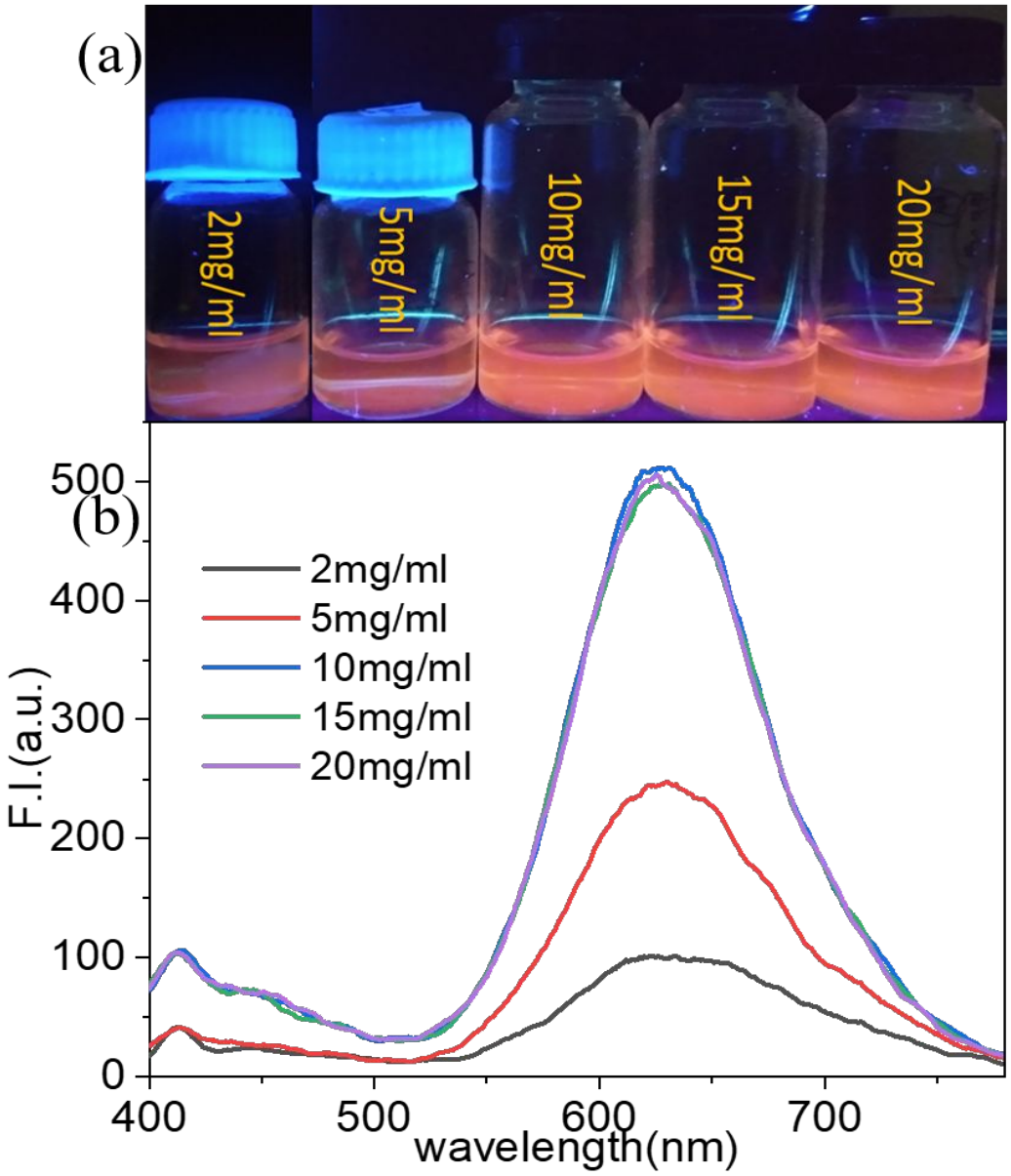

Fig. S1. (a) Vials image of β-CD-GSH-CuNCs with varying amounts of β-CD showing the intensity of fluorescent colour under the UV irradiation at 365 nm. (b) Fluorescence spectral change in β-CD-GSH-CuNCs with different amounts of β-CD.

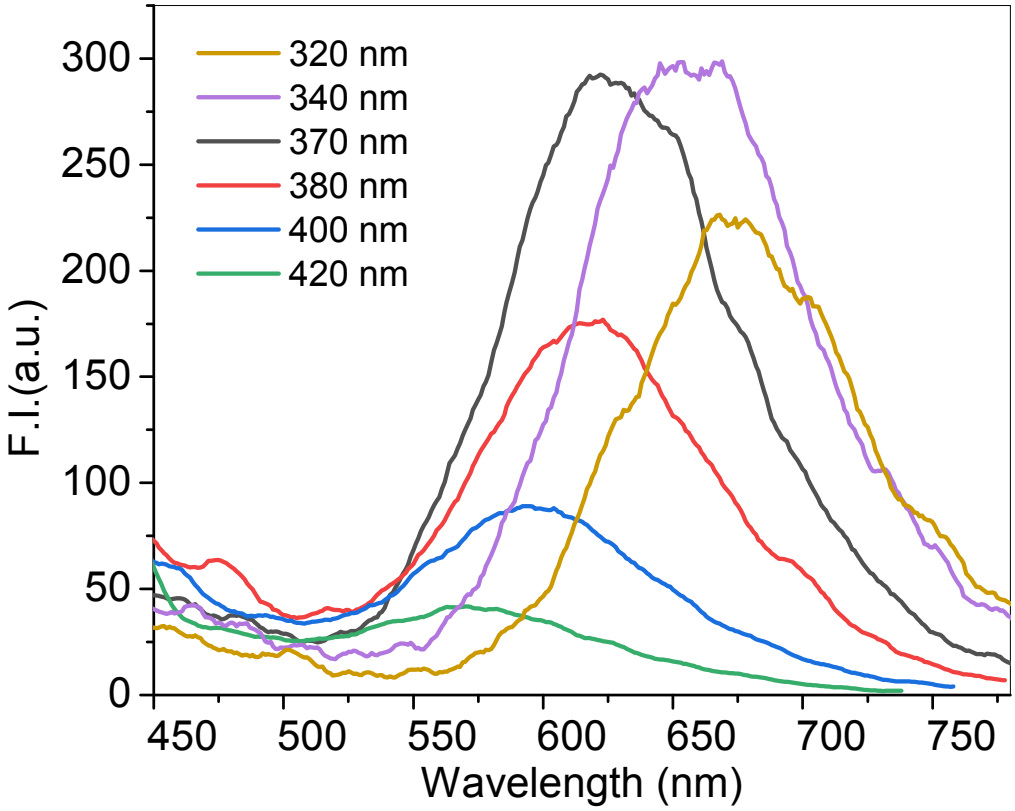

Fig. S2. The emission spectra of β-CD-GSH-CuNCs at different excitation wavelengths.

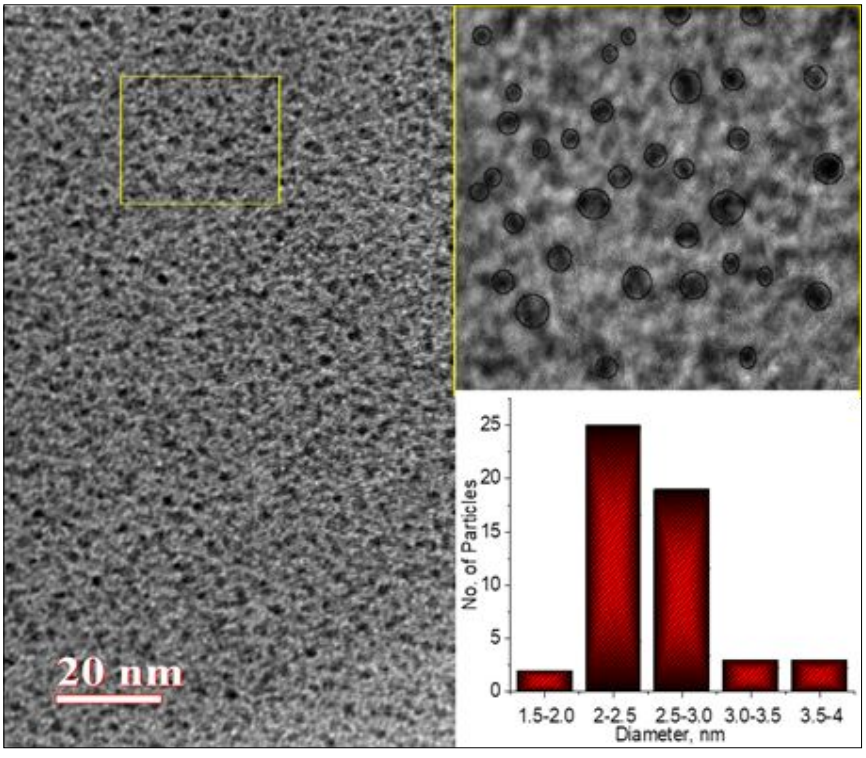

Fig. S3. (a) HR-TEM image of β-CD-GSH-CuNCs and (b) enlarged particles highlighted by circle. (c) Statistical analysis histogram of calculated particles.

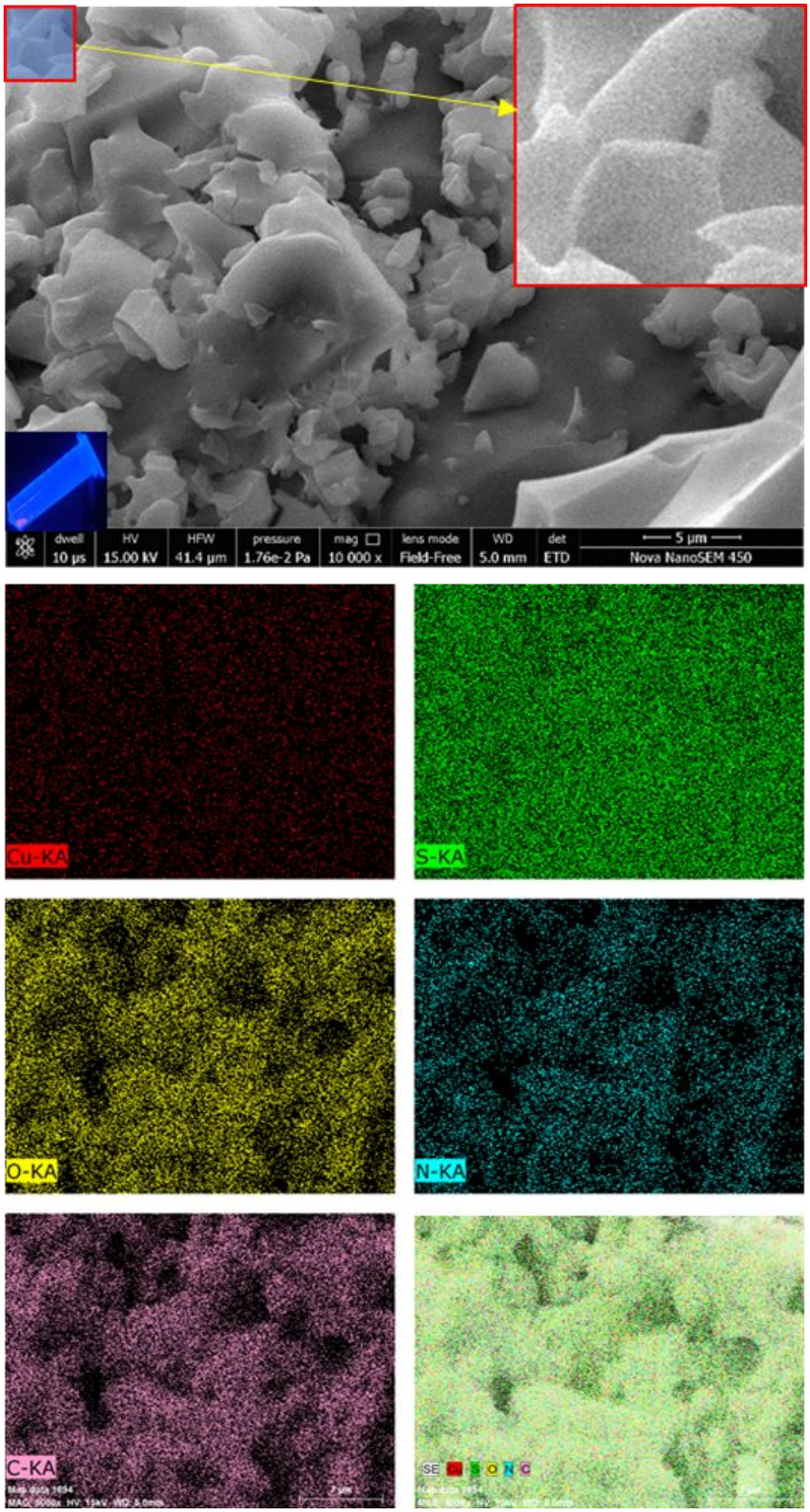

Fig. S4. FE-SEM image of the isolated solid (inset) β-CD-GSH-CuNCs and the EDX elemental mapping showing the presence of Cu, S, O, N and C elements.

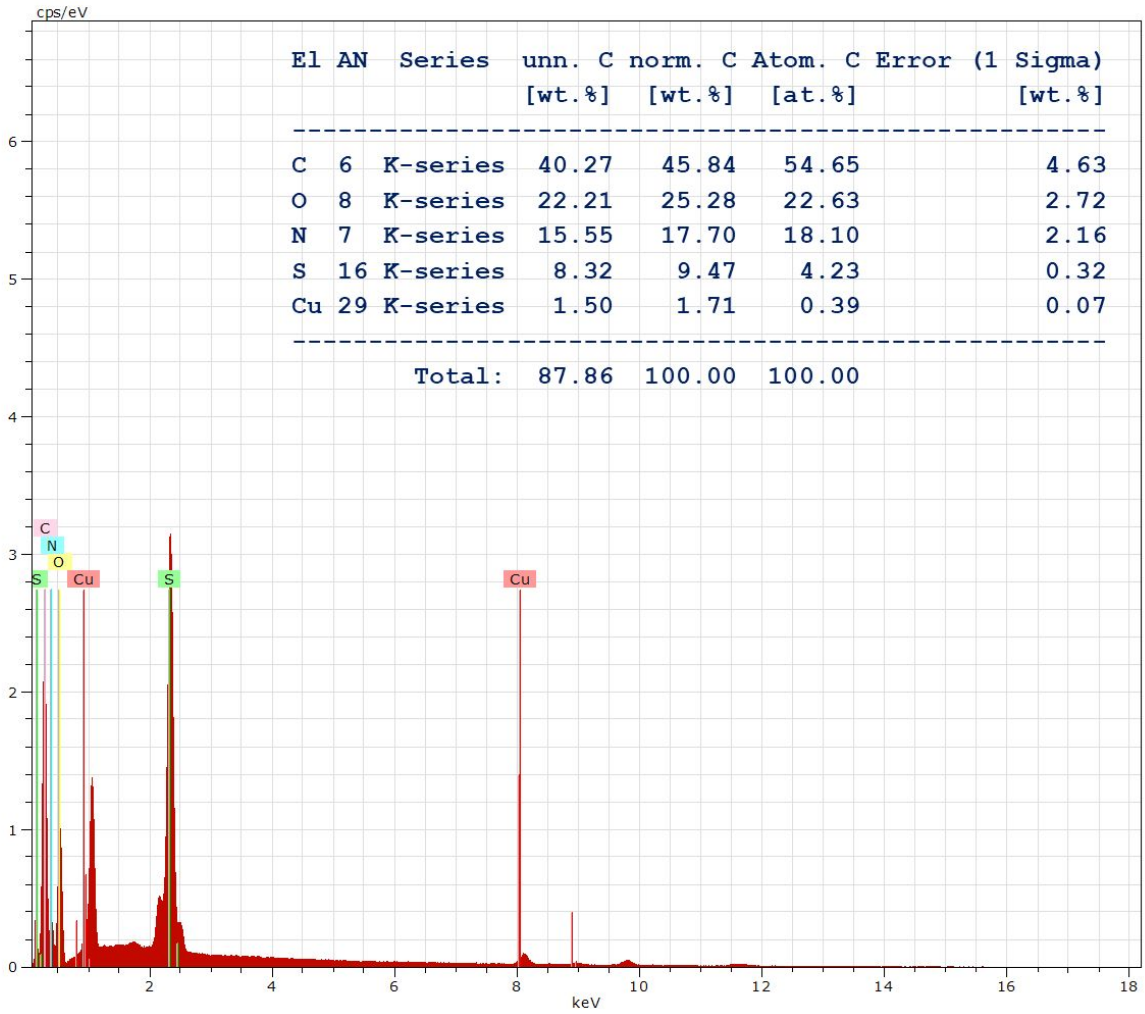

Fig. S5. Energy-dispersive X-ray (EDX) spectrum for the elemental characterisation of β-CD-GSH-CuNCs.

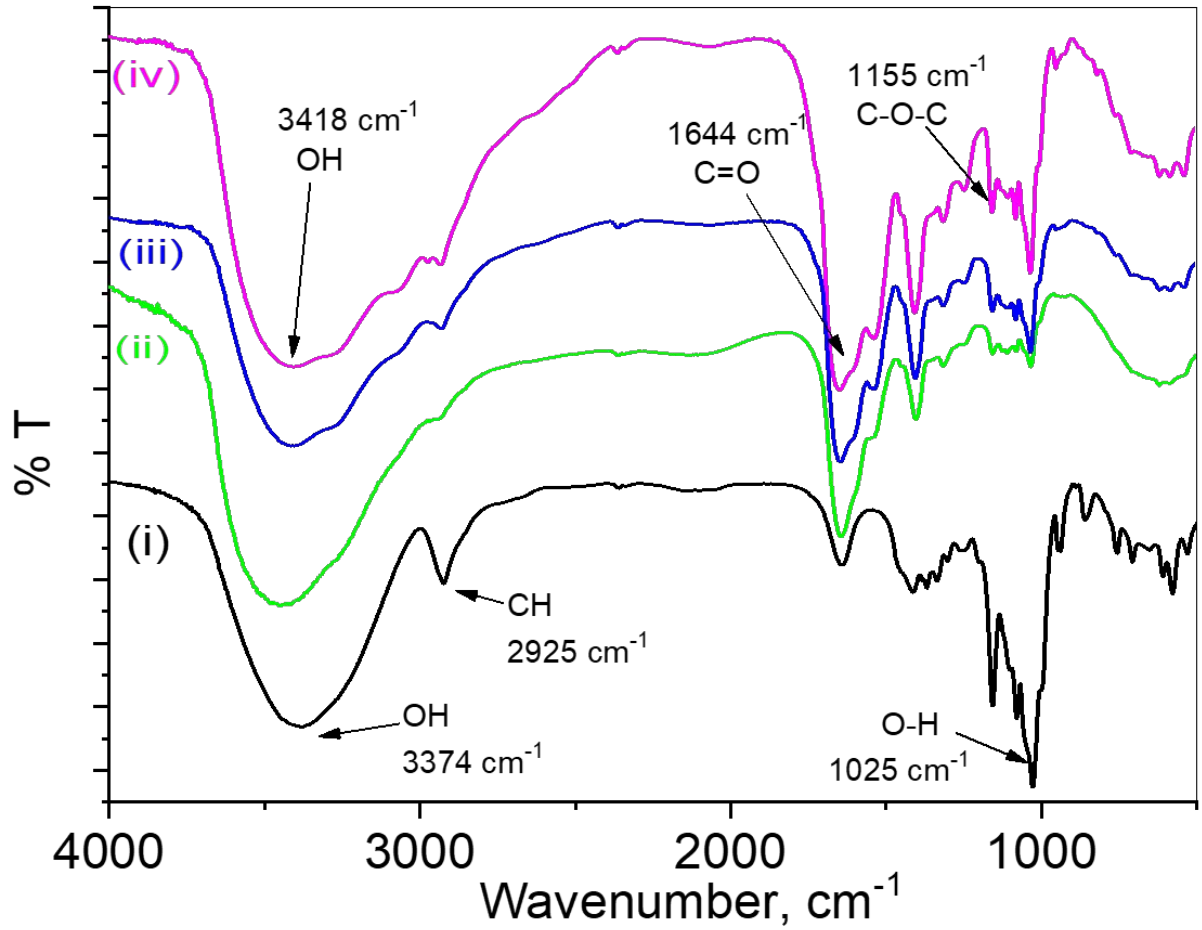

Fig. S6. Infrared spectra of (i) β-CD, (ii) β-CD-GSH-CuNCs, (iii) β-CD-GSH-CuNCs@PLP and (iv) β-CD-GSH-CuNCs@PLP in presence of Al^{3+}.

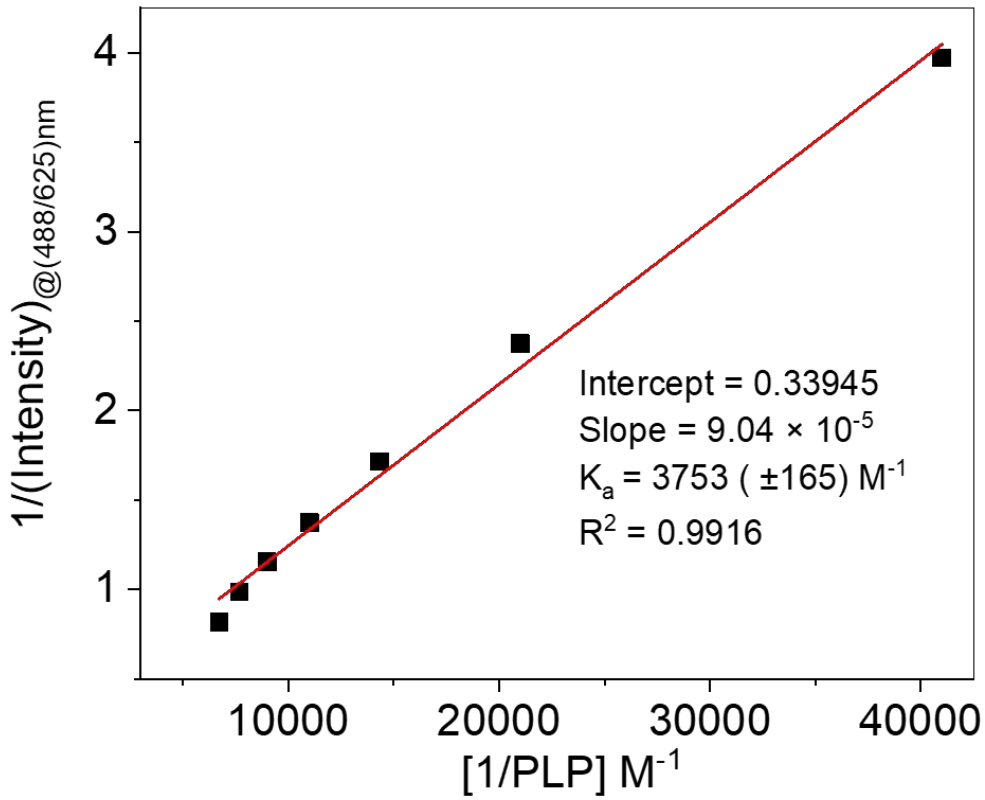

Fig. S7. The Benesi-Hildebrand plot of PLP with β-CD-GSH-CuNCs for calculating binding constant.

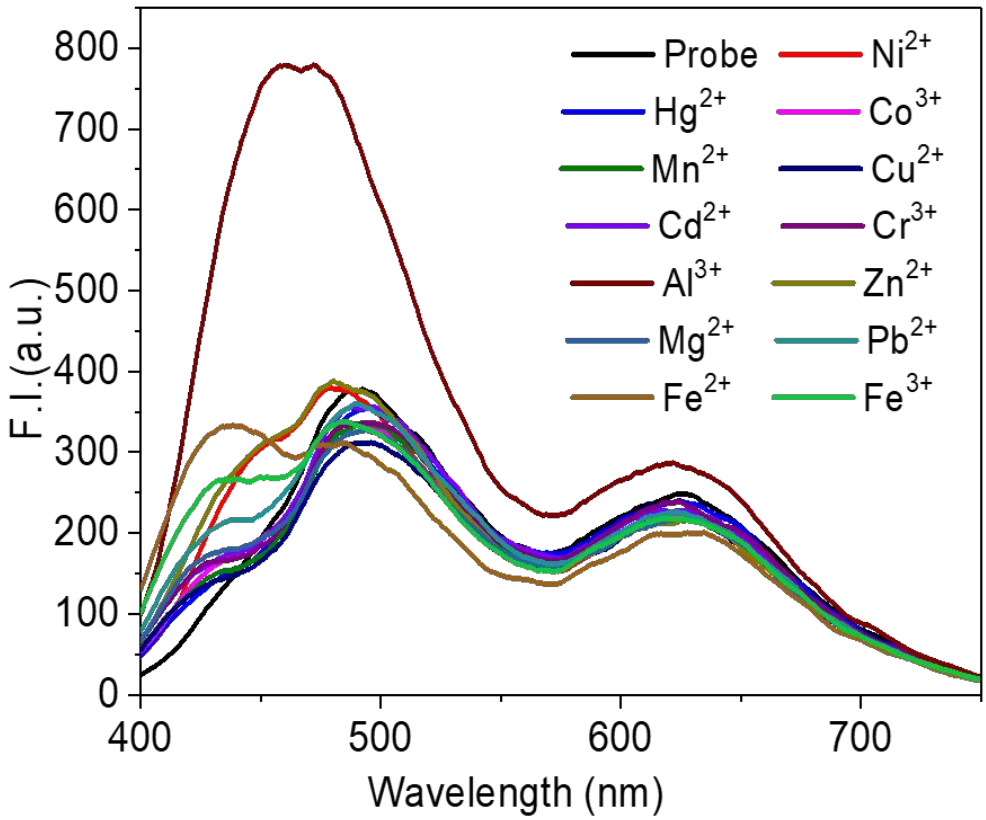

Fig. S8. Emission spectra of β-CD-GSH-CuNCs@PLP in presence of various metal ions.

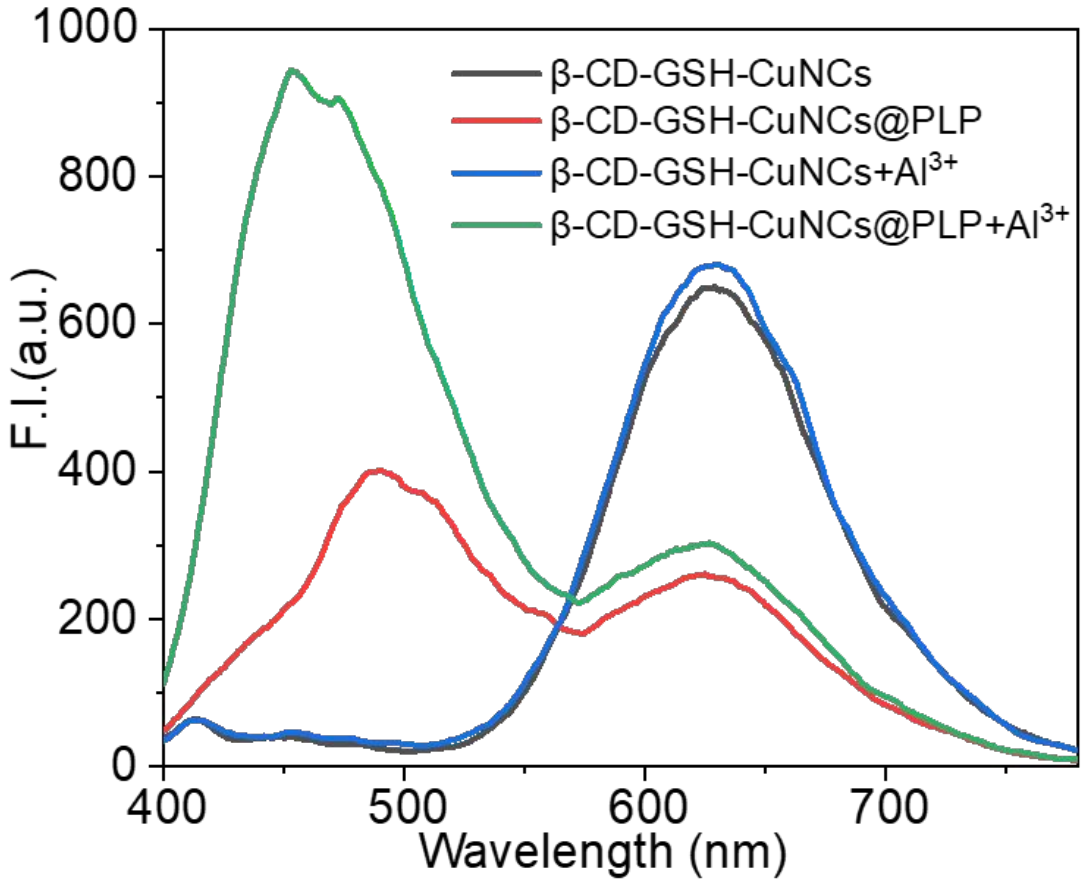

Fig. S9. Fluorescence emission spectra of β-CD-GSH-CuNCs, β-CD-GSH-CuNCs@PLP, β-CD-GSH-CuNCs +Al^{3+} without PLP and β-CD-GSH-CuNCs@PLP with Al^{3+}.

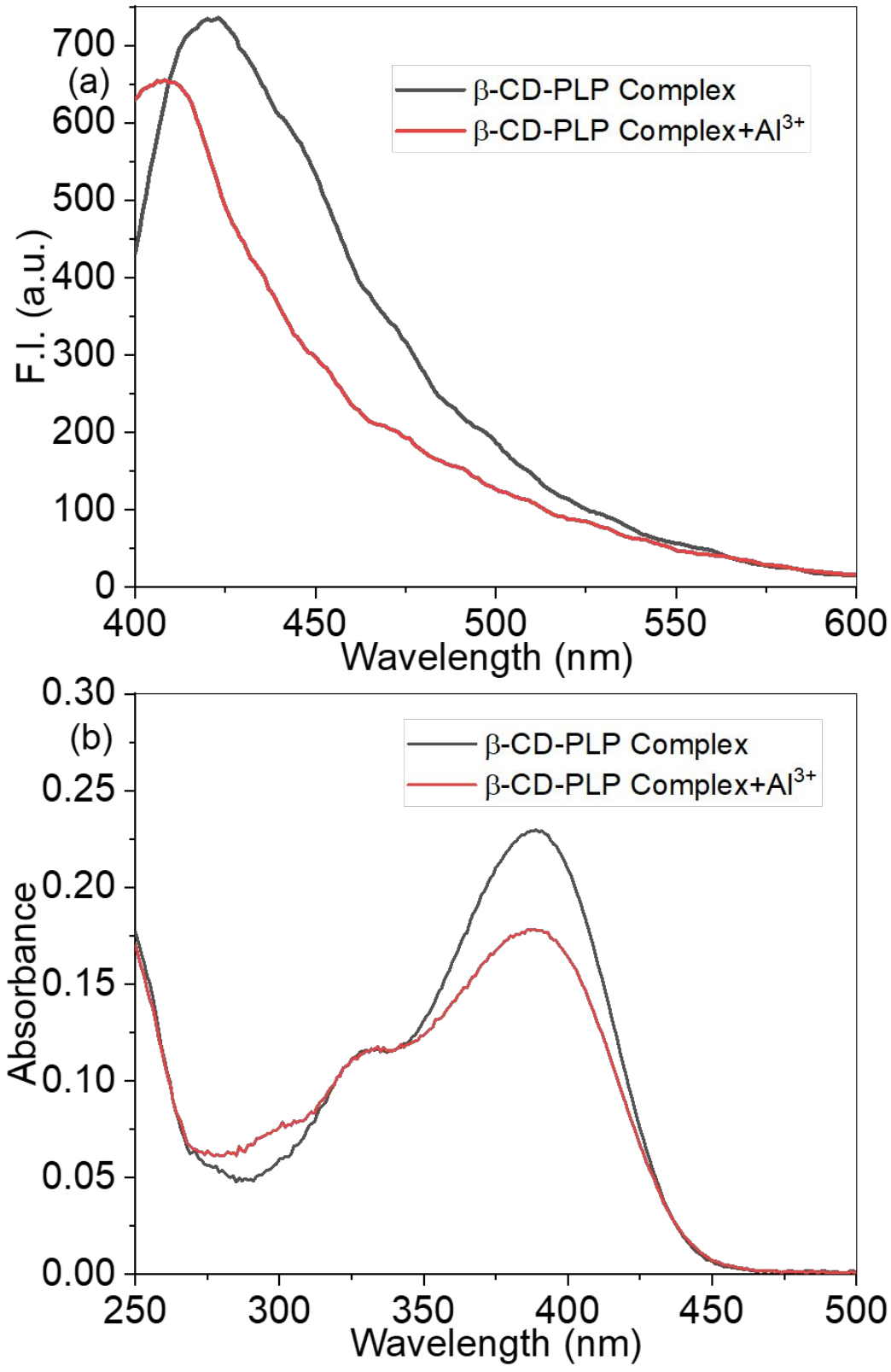

Fig. S10. (a) Emission and (b) UV-Vis spectral changes of β-CD/PLP inclusion complex after addition of Al^{3+} (1.76×10^{-5} M).

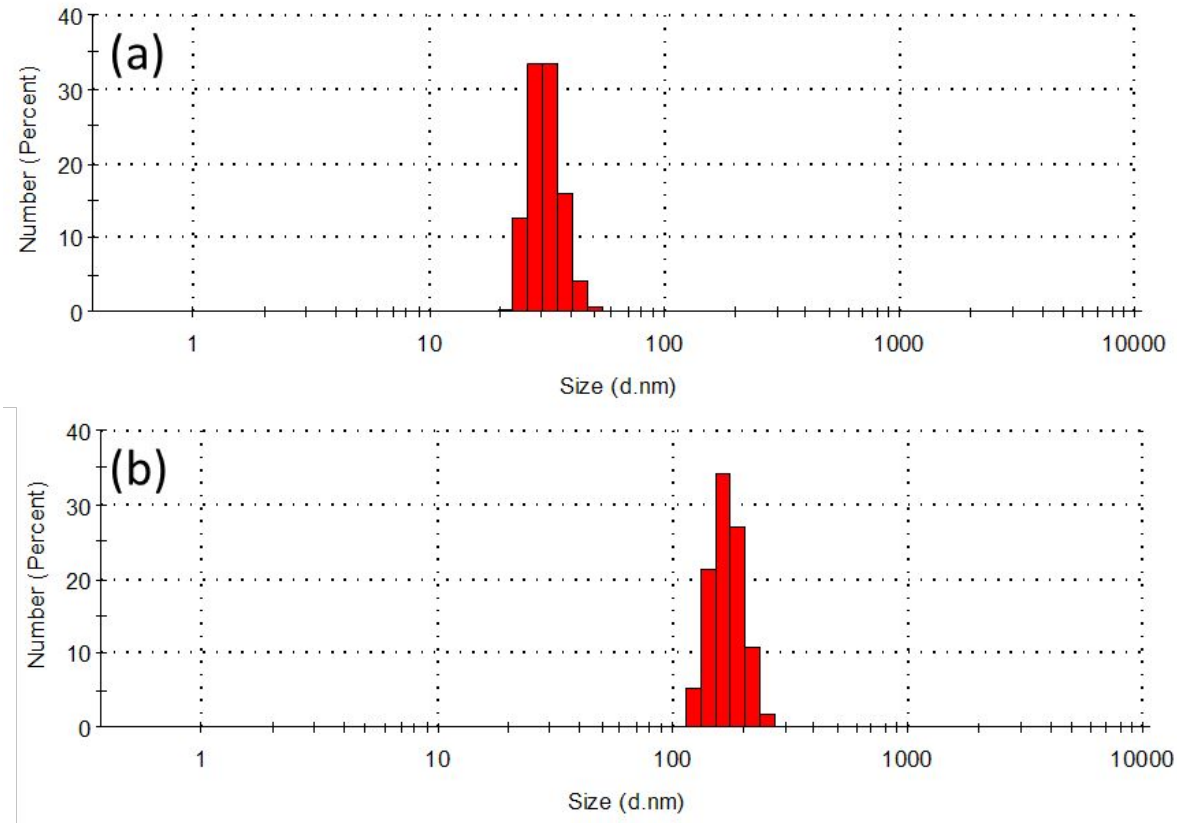

Fig. S11. DLS results of β-CD-GSH-CuNCs@PLP in the absence (a) and presence of Al^{3+} (b).

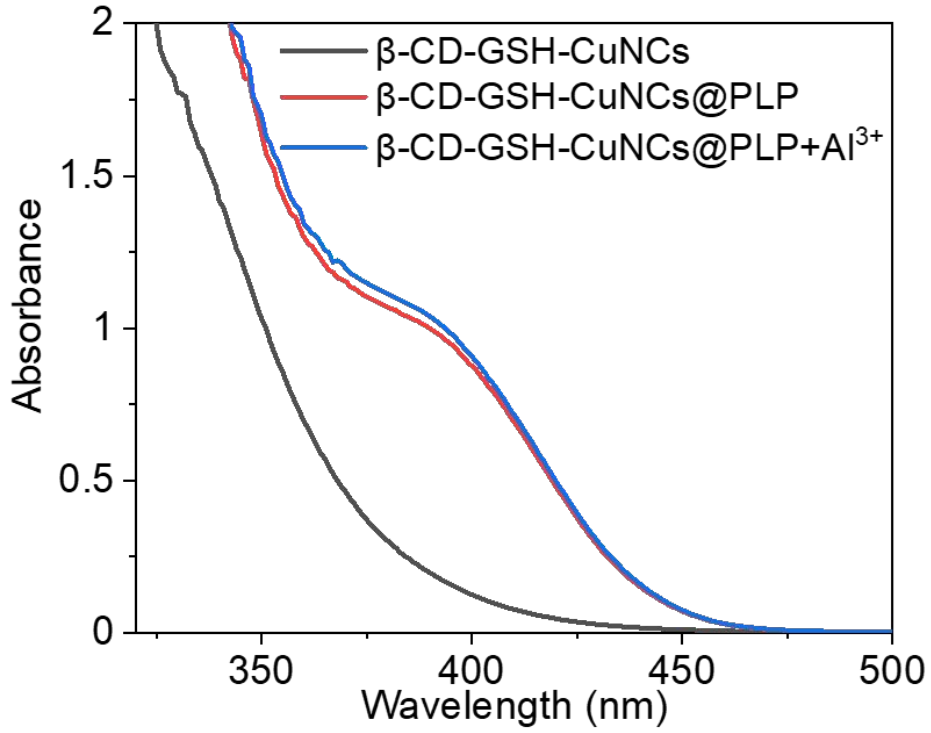

Fig. S12. UV-Vis spectrum of β-CD-GSH-CuNC, β-CD-GSH-CuNCs@PLP and β-CD-GSH-CuNCs@PLP with Al^{3+}.

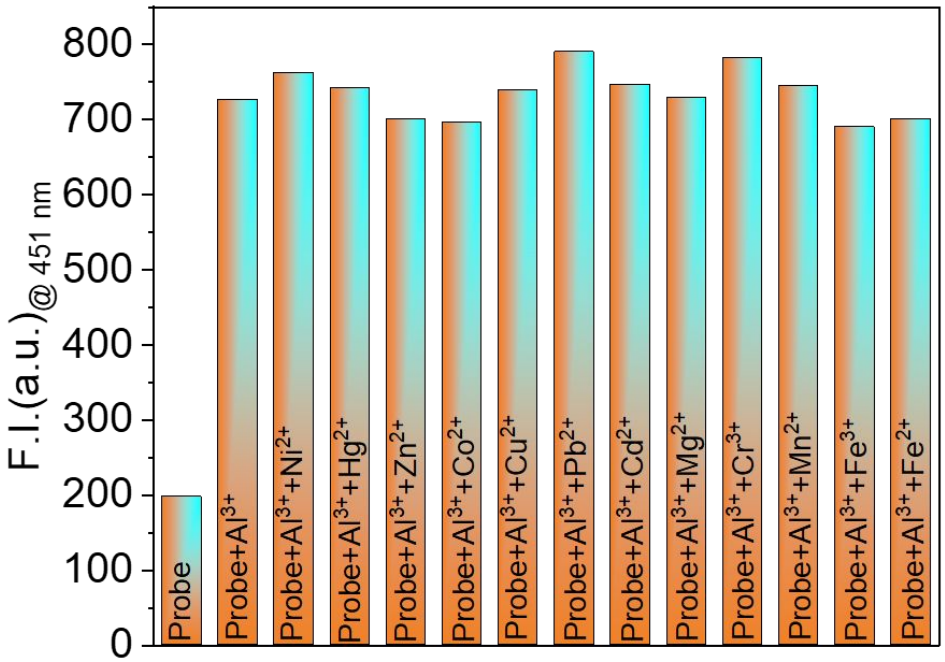

Fig. S13. Bar graph shows Al^{3+} ion detection in the presence of various interfering metal ions.

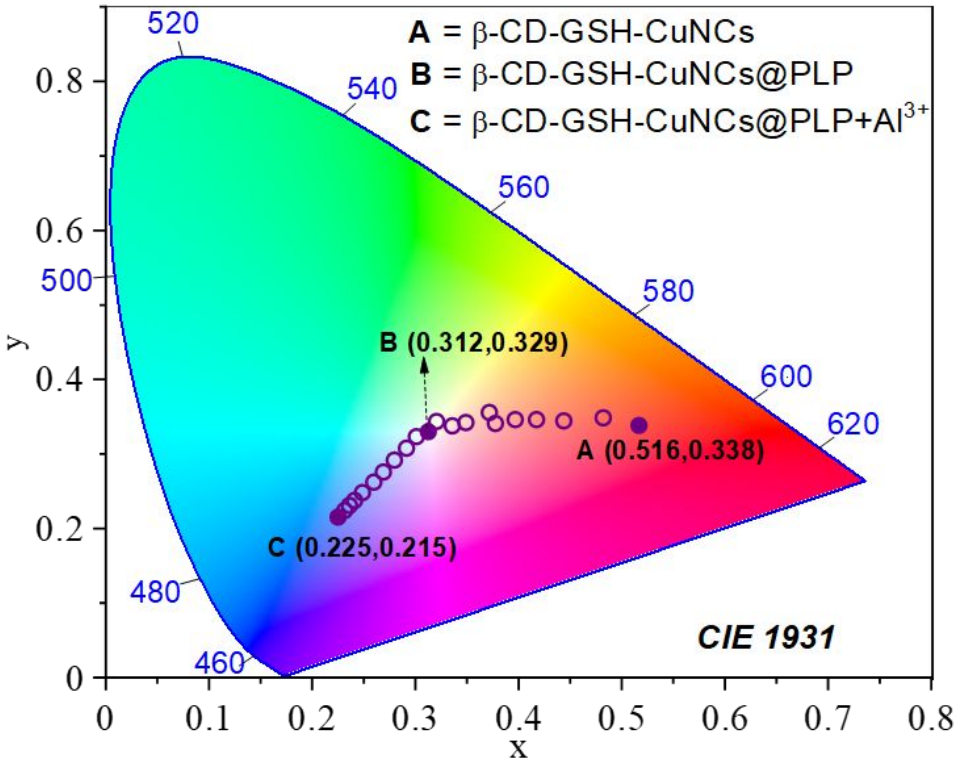

Fig. S14. CIE 1931 chromaticity diagram showing point (A) the colour coordinates of β-CD-GSH-CuNCs, point (B) the colour coordinates when the PLP concentration was 2×10^{-4} M, and point (C) the colour coordinates when the Al^{3+} (2.4×10^{-6} M) was added to *in situ* generated β-CD-GSH-CuNCs@PLP.

Table S1. Comparison with other recently published nanosensors for the detection of Al^{3+} ions.

Fluorescent nanosensors	Medium	LOD (μM)	Ref.
Mercaptosuccinic acid stabilized AgAu alloy nanoclusters (MSA−AgAu NCs)	H_2O	0.8	1
Gallic acid-functionalized AgNPs	H_2O	0.92	2
Xylenol orange functionalized gold nanoparticles (XO-AuNPs)	H_2O	0.04	3
Cysteamine-capped copper nanoclusters(Cys-CuNCs)	acetic-acetate buffer	26.7	4
Pyridoxal derivative functionalized gold nanoparticles	H_2O	0.51	5
Dithiothreitol capped copper nanoclusters(DTT-CuNCs)	HAc-NaAc buffer	0.01	6
glutathione (GSH)-capped Au NCs(GSH)-capped Au NCs)	acetate buffer	20	7
Polyacrylate functionalized gold nanoparticles (PAA-AuNPs)	H_2O	2	8
N-(2-hydroxynaphthylidene)-2-aminoethanethiol capped AuNPs (HNAET–AuNPs)	H_2O	0.29	9
Glutathione-silver nanoclusters (AgNCs)	H_2O	0.1	10
β-CD-GSH-CuNCs@PLP	**H_2O**	**0.187**	**Our study**

References

(1) Zhou, T.-Y.; Lin, L.-P.; Rong, M.-C.; Jiang, Y.-Q.; Chen, X. Silver–Gold Alloy Nanoclusters as a Fluorescence-Enhanced Probe for Aluminum Ion Sensing. *Anal. Chem.* **2013**, *85* (20), 9839-9844.

(2) Ghodake, G.; Shinde, S.; Kadam, A.; Saratale, R. G.; Saratale, G. D.; Syed, A.; Shair, O.; Alsaedi, M.; Kim, D.-Y. Gallic Acid-Functionalized Silver Nanoparticles as Colorimetric and Spectrophotometric Probe for Detection of Al^{3+} in Aqueous Medium. *J. Ind. Eng. Chem.* **2020**, *82*, 243-253.

(3) Garg, N.; Bera, S.; Ballal, A. Spr Responsive Xylenol Orange Functionalized Gold Nanoparticles-Optical Sensor for Estimation of Al^{3+} in Water. *Spectrochim. Acta, Part A* **2020**, *228*, 117701.

(4) Boonmee, C.; Promarak, V.; Tuntulani, T.; Ngeontae, W. Cysteamine-Capped Copper Nanoclusters as a Highly Selective Turn-on Fluorescent Assay for the Detection of Aluminum Ions. *Talanta* **2018**, *178*, 796-804.

(5) Bothra, S.; Kumar, R.; Sahoo, S. K. Pyridoxal Derivative Functionalized Gold Nanoparticles for Colorimetric Determination of Zinc(II) and Aluminium(III). *RSC adv.* **2015**, *5*, 97690-97695.

(6) Hu, X.; Mao, X.; Zhang, X.; Huang, Y. One-Step Synthesis of Orange Fluorescent Copper Nanoclusters for Sensitive and Selective Sensing of Al^{3+} Ions in Food Samples. *Sensors Actuators B: Chem.* **2017**, *247*, 312-318.

(7) Luo, P.; Zheng, Y.; Qin, Z.; Li, C.; Jiang, H.; Wang, X. Fluorescence Light up Detection of Aluminium Ion and Imaging in Live Cells Based on the Aggregation-Induced Emission Enhancement of Thiolated Gold Nanoclusters. *Talanta* **2019**, *204*, 548-554.

(8) Kumar, A.; Bhatt, M.; Vyas, G.; Bhatt, S.; Paul, P. Sunlight Induced Preparation of Functionalized Gold Nanoparticles as Recyclable Colorimetric Dual Sensor for Aluminum and Fluoride in Water. *ACS Appl. Mater. Interfaces* **2017**, *9*, 17359-17368.

(9) Huang, P.; Li, J.; Liu, X.; Wu, F. Colorimetric Determination of Aluminum(III) Based on the Aggregation of Schiff Base-Functionalized Gold Nanoparticles. *Microchim. Acta* **2016**, *183*, 863-869.

(10) Liu, X.; Shao, C.; Chen, T.; He, Z.; Du, G. Stable Silver Nanoclusters with Aggregation-Induced Emission Enhancement for Detection of Aluminum Ion. *Sensors Actuators B: Chem.* **2019**, *278*, 181-189.

****